Epitaxial growth of ferromagnetic $Co_xFe_{4-x}N$ thin films on $SrTiO_3$(001) and magnetic properties

Tatsunori Sanai, Keita Ito, Kaoru Toko, and Takashi Suemasu

Institute of Applied Physics, University of Tsukuba, Tsukuba, Ibaraki 305-8573, Japan

Keywords: A3. Molecular beam epitaxy, B2. Ferromagnetic materials, B1. $Co_xFe_{4-x}N$, B1. $SrTiO_3$

Corresponding author: T. Suemasu

Institute of Applied Physics, University of Tsukuba, Tsukuba, Ibaraki 305-8573, Japan

TEL/FAX: +81-29-853-5111, Email: suemasu@bk.tsukuba.ac.jp

We formed $Co_xFe_{4-x}N$ ($0 \leq x \leq 2.9$) epitaxial thin films on $SrTiO_3$(001) substrates by molecular beam epitaxy supplying solid Co and Fe and a radio frequency N_2 plasma, simultaneously. The composition ratio of Co/Fe in $Co_xFe_{4-x}N$ was controlled by changing the weight ratio of Co to Fe flakes in the crucible of the Knudsen cell used. Epitaxial growth of $Co_xFe_{4-x}N$ thin films were confirmed by reflection high-energy electron diffraction and θ-2θ X-ray diffraction patterns. Magnetization versus magnetic field curves measured at room temperature using a vibrating sample magnetometer showed that the axis of easy magnetization was changed from [100] to [110] with increasing x in $Co_xFe_{4-x}N$.

1. Introduction

Spintronics has attracted significant attention in recent years. Techniques of spin injection, control and detection are required to achieve spintronic devices. Therefore, highly spin-polarized ferromagnetic materials are of great importance as spin sources. Numerous different types of half metals and hetero junctions have been studied extensively [1-4]. Among such materials, we have focused on cubic perovskite 3*d* ferromagnetic nitrides such as Fe_4N and Co_4N [5-10]. Fe_4N has been extensively studied over the past few years. It has a cubic perovskite lattice structure, wherein a nitrogen atom is located in the body center of the fcc-Fe lattice. Spin polarization of the density of states (P) at the Fermi level (E_F) and spin asymmetry of the electrical conductivity were calculated to be −0.6 and −1.0, respectively [11]. There have been a few reports on the inverse tunnel magnetoresistance of −75% in CoFeB/MgO/Fe_4N magnetic tunnel junctions and negative anisotropic magnetoresistance in Fe_4N films at room temperature (RT) [12-15]. Therefore, Fe_4N is considered an appropriate material for application in spintronics devices. A recent theoretical calculation predicts that Co_4N has a larger negative polarization than Fe_4N [16]. In particular, recent first-principles calculation indicating that P was estimated to be −1.0 in Co_3FeN has renewed interest in this material [17]. $Co_xFe_{4-x}N$ also has a cubic perovskite lattice structure, which is the same as those of Fe_4N and Co_4N, with a nitrogen atom occupying the body center such as. However, there has been no data about whether the Co atoms occupy the face-centered positions or corner positions. We therefore expect that $Co_xFe_{4-x}N$ alloy is very promising for application in spintronics devices. However, there had been no reports so far on epitaxial growth of $Co_xFe_{4-x}N$ thin films. Very recently, we successfully formed epitaxial growth of $Co_xFe_{4-x}N$ films on $SrTiO_3$(STO)(001) substrates by molecular beam epitaxy (MBE) [18]. The epitaxial orientation of $Co_xFe_{4-x}N$ on STO(001) is $Co_xFe_{4-x}N$ (001)//STO(001) with $Co_xFe_{4-x}N$ [100] or [010] // STO[100]. However, there have been no reports thus far on the magnetic properties of $Co_xFe_{4-x}N$ thin films. In this work, we aimed to form $Co_xFe_{4-x}N$ thin films, and measured the magnetic properties of the films at RT.

2. Experimental procedures

An ion-pumped MBE system equipped with a high-temperature Knudsen cell for Fe and Co sources, and a radio-frequency (RF) N_2 plasma for N was used [6,7,18]. Prior to the growth, the STO(001) substrates were immersed into a buffered HF solution to obtain an atomically flat surface [19]. The lattice mismatch between Fe_4N and STO is 2.8% [20]. Co and Fe flakes were placed into the same crucible. Various weight ratios of Co/Fe in the crucible were used including 0:1 (sample A), 0.5:1 (sample B), 1:1 (sample C), 3:1 (sample D) and 5.6:1 (sample E). During the growth of these samples, the temperature of the STO substrate was kept at 450 °C, and the deposition rate of Co plus Fe was set to be approximately 0.5 nm/min. The flow rate of the N_2 gas was fixed at 1.0 sccm, and the input power to the RF plasma was 140 W. The pressure inside the chamber was approximately 1×10^{-4} Torr during film growth. Sample preparation was summarized in Table 1.

The crystalline quality of samples A-E was evaluated by reflection high-energy electron diffraction (RHEED), θ-2θ X-ray diffraction (XRD) using Cu K_α X-ray, and atomic force microscopy (AFM). The composition ratio of Co/Fe in the films was determined by energy dispersive X-ray spectroscopy (EDX) using an accelerating voltage of 10 kV with a spot size of 30 μm and by Rutherford back scattering spectrometry (RBS) using a He ion beam with an acceleration voltage of 2.3 MeV. Magnetization versus magnetic field curves were measured on approximately 10-mm-squared samples at RT using a vibrating sample magnetometers (VSM) in the range of external magnetic field H (-1 T $\leq H \leq$ 1 T).

3. Results and discussion

Figures 1(a)-1(e) show the RHEED patterns observed along the STO[100] azimuth of samples A-E, respectively. Streaky RHEED patterns were observed except for the spotty patterns for samples B and C. The RBS depth profiles of Co, Fe, and N atoms revealed that the composition ratio of $(CoFe)_4N$ in sample D was $Co_{2.3}Fe_{1.7}N$ [18]. Using sample D as a reference, the composition ratios were determined from the signal intensities of Co K_α (6.924 keV) and Fe K_β (7.057 keV) X-rays in the EDX spectra for samples B, C and E. We evaluated the composition ratio of Co/Fe for samples B, C and E to be $Co_{0.4}Fe_{3.6}N$,

$Co_{1.2}Fe_{2.8}N$ and $Co_{2.9}Fe_{1.1}N$, respectively, as summarized in Table 1. Detailed procedure was given in our previous report [18].

The out-of-plane θ-2θ XRD patterns of samples A-E are shown in Figs. 2(a)-2(e), respectively. The diffraction peaks of $(CoFe)_4N(001)$, (002) and (004) were observed. With increasing weight ratio of Co to Fe in the crucible, these peaks shifted to a higher angle, meaning that the out-of-plane lattice constants decrease with increasing Co/Fe ratio in $Co_xFe_{4-x}N$.

Figures 3(a) and 3(b) present the AFM images of samples C and E, respectively. The root-mean-square (rms) roughness values of these samples were 0.98 and 1.74 nm, respectively. With respect to the $Co_xFe_{4-x}N$ layer thicknesses of these samples, these rms values are not small. Thus, further studies are mandatory to achieve $Co_xFe_{4-x}N$ layers with much smoother surfaces.

Next, we discuss the magnetic properties of the grown films. Figures 4(a)-4(e) present the incident H angle dependence of the ratio of remanent magnetization (M_r) to saturation magnetization (M_s), namely M_r/M_s for samples A-E, respectively, at RT. External H was applied between the [110] and [1-10] azimuths of $Co_xFe_{4-x}N$ parallel to the sample surface. The crystalline magnetic anisotropy was observed. Owing to the 10-mm-squared samples, shape magnetic anisotropy is considered to be negligibly small. M_r differs depending on the directions of applied external H. For sample A, Fe_4N, the in-plane [100] direction is an easy magnetization axis in Fig. 4(a). When the Co/Fe ratio increases a little in sample B, $Co_{0.4}Fe_{3.6}N$, the easy magnetization axis remained the same as in Fig. 4(b). But when the Co/Fe ratio increased further in samples C-E, the axis of easy magnetization drastically changed from [100] to [110] or [1-10] direction. These results indicate that the magnetic anisotropy changed depending on the Co/Fe ratio of the film. The reason for this change is not made clear at present. Thus, further studies are required to clarify the mechanism that explains this change.

4. Conclusions

We have succeeded in growing $Co_xFe_{4-x}N$ ($0 \leq x \leq 2.9$) thin films epitaxially on STO(001) substrates by MBE supplying solid Co, Fe, and RF-N_2, simultaneously. VSM measurements revealed that the axis of easy magnetization was [100] for Fe_4N and $Co_{0.4}Fe_{3.6}N$. When the Co/Fe ratio increased further, the axis of easy magnetization was changed from [100] to [110].

Acknowledgements

The authors thank Dr. Y. Imai of the National Institute of Advanced Industrial Science and Technology (AIST), Tsukuba, for useful discussions. Magnetic characterizations were performed with the cooperation of Dr. H. Yanagihara.

References

[1] M. Bowen, M. Bibes, A. Barthe´le´my, J.-P. Contour, A. Anane, Y. Lemaıˆtre, A. Fert, Appl. Phys. Lett. 82 (2003) 233.

[2] J. M. D. Coey, M. Venkatesan, J. Appl. Phys. 91 (2002) 8345.

[3] T. Ishikawa, S. Hakamata, K. Matsuda, T. Uemura, M. Yamamoto, J. Appl. Phys. 103 (2008) 07A919.

[4] S. Yuasa, T. Nagahama, A. Fukushima, Y. Suzuk, K. Ando, Nat. Mater. 3 (2004) 868.

[5] A. Narahara, K. Ito, T. Suemasu, Y. K. Takahash, A. Rajanikanth, K. Hono, Appl. Phys. Lett 94 (2009) 202502.

[6] K. Ito, G. H. Lee, H. Akinaga, T. Suemasu, J. Cryst. Growth 322 (2011) 63.

[7] K. Ito, K. Harada, K. Toko, H. Akinaga, T. Suemasu, J. Cryst. Growth 336 (2011) 40.

[8] K. Ito, G. H. Lee, K. Harada, M. Suzuno, T. Suemasu, Y. Takeda, Y. Saitoh, M. Ye, A Kimura, H. Akinaga, Appl. Phys. Lett. 98 (2011) 102507.

[9] K. Ito, K. Harada, K. Toko, M.Ye, A. Kimura, Y. Takeda, Y. Saitoh, T. Suemasu, Appl. Phys. Lett. 99 (2011) 252501.

[10] K. Ito, K. Okamoto, K. Harada, T. Sanai, K. Toko, S. Ueda, Y. Imai, T. Okuda, K. Miyamoto, A. Kimura, T. Suemasu, J. Appl. Phys. 112 (2012) 013911.

[11] S. Kokado, N. Fujima, K. Harigaya, H. Shimizu, A. Sakuma, Phys. Rev. B 73 (2006) 172410.

[12] Y. Komasaki, M. Tsunoda, S. Isogami, M. Takahashi, J. Appl. Phys. 105 (2009) 07C928.

[13] M. Tsunoda, Y. Komasaki, S. Kokado, S. Isogami, C. C. Chen, M. Takahashi, Appl. Phys. Express 2 (2009) 083001.

[14] M. Tsunoda, H. Takahashi, S. Kokado, Y. Komasaki, A. Sakuma, M. Takahashi, Appl. Phys. Express 3 (2010) 113003.

[15] K. Ito, K. Kabara, H. Takahashi, T. Sanai, K. Toko, T. Suemasu, M. Tsunoda, Jpn. J. Appl. Phys. 51 (2012) 068001.

[16] Y. Imai, Y. Takahashi, T. Kumagai, J. Magn. Magn. Mater. 322 (2010) 2665.

[17] Y. Takahashi, Y. Imai, T. Kumagai, J. Magn. Magn. Mater. 323 (2011) 2941.

[18] T. Sanai, K. Ito, K. Toko, T. Suemasu, J. Cryst. Growth 357 (2012) 53.

[19] M. Kawasaki, K. Takahashi, T. Maeda, R. Tsuchiya, M. Shinohara, O. Ishiyama, T. Yonezawa, M. Yoshimoto, H. Koinuma, Science 266 (1994) 1540.

[20] S. Atiq, H. S. Ko, S. A. Siddiqi, S. C. Shin, Appl. Phys. Lett. 92 (2008) 222507.

Fig. 1 RHEED patterns of samples A (a), B (b), C (c), D (d), and E (e), observed along the STO[100] azimuth.

Fig. 2. Out-of-plane θ–2θ XRD patterns of samples A (a), B (b), C (c), D (d), and E (e).

Fig. 3. AFM images of samples C (a) and E (b).

Fig. 4. Incident H angle dependence of M_r/M_s for samples A (a), B (b), C (c), D (d), and E (e), measured at RT. External H was applied between the [100] and [1-10] azimuths of $Co_xFe_{4-x}N$ parallel to the sample surface.

Table 1. Sample preparation: grown layer thicknesses, and composition ratios of Co/Fe in $Co_xFe_{4-x}N$ are shown.

Sample	Thickness (nm)	$Co_xFe_{4-x}N$
A	10	Fe_4N
B	33	$Co_{0.4}Fe_{3.6}N$
C	29	$Co_{1.2}Fe_{2.8}N$
D	22	$Co_{2.4}Fe_{1.6}N$
E	21	$Co_{2.9}Fe_{1.1}N$

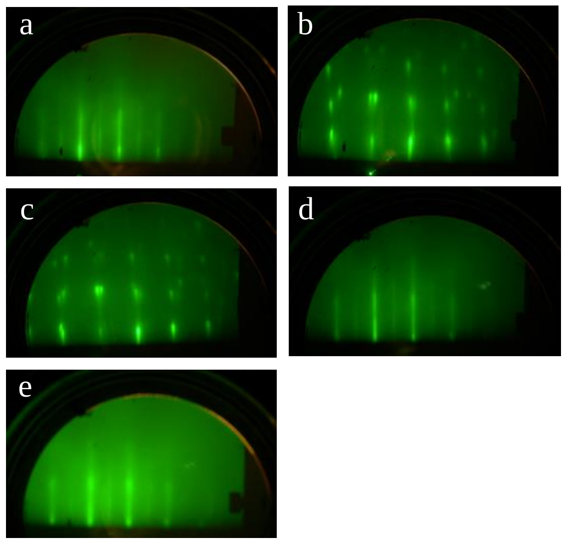

Fig. 1

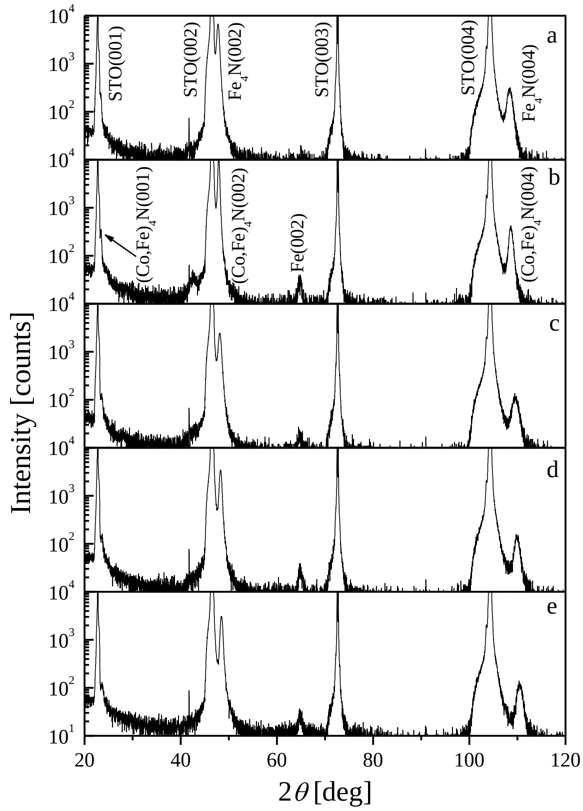

Intensity [counts]
2θ [deg]
STO(001)
STO(002)
Fe4N(002)
STO(003)
STO(004)
Fe4N(004)
(Co,Fe)4N(001)
(Co,Fe)4N(002)
Fe(002)
(Co,Fe)4N(004)
a
b
c
d
e

Fig. 2

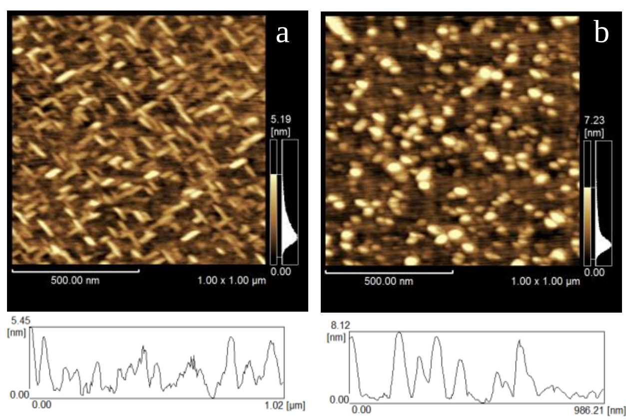

a
5.19
[nm]
0.00
500.00 nm
1.00 x 1.00 µm
5.45
[nm]
0.00
0.00
1.02 [µm]
b
7.23
[nm]
0.00
500.00 nm
1.00 x 1.00 µm
8.12
[nm]
0.00
0.00
986.21 [nm]

Fig. 3

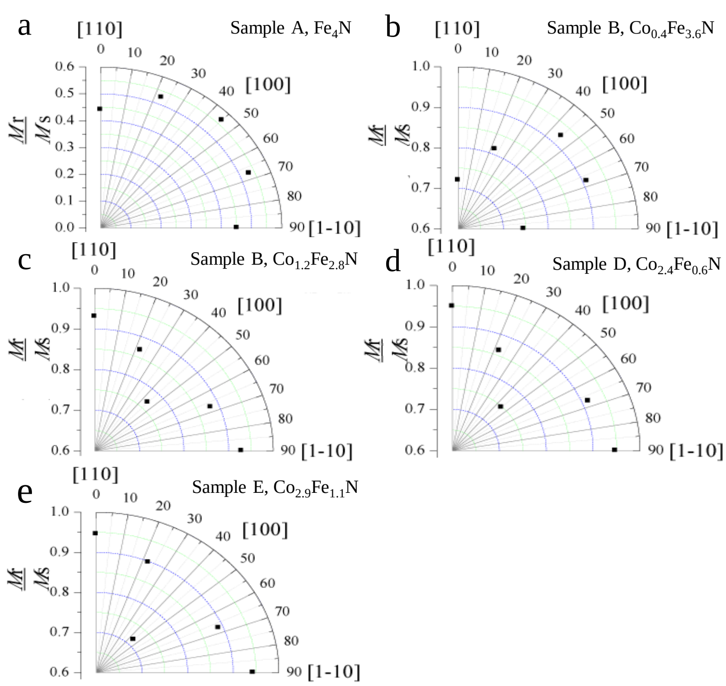
a
Sample A, Fe$_4$N
b
Sample B, Co$_{0.4}$Fe$_{3.6}$N
c
Sample B, Co$_{1.2}$Fe$_{2.8}$N
d
Sample D, Co$_{2.4}$Fe$_{0.6}$N
e
Sample E, Co$_{2.9}$Fe$_{1.1}$N
[110]
[100]
[1-10]
Mr/Ms

Fig. 4